Annals of Botany **99**: 593–607, 2007
doi:10.1093/aob/mcm002, available online at www.aob.oxfordjournals.org

OXFORD JOURNALS
OXFORD UNIVERSITY PRESS

Ultrastructural Evidence for a Dual Function of the Phloem and Programmed Cell Death in the Floral Nectary of *Digitalis purpurea*

KARL PETER GAFFAL[1,*], GUDRUN JOHANNA FRIEDRICHS[1] and STEFAN EL-GAMMAL[2]

[1]*Institut für Biologie, Lehrstuhl für Pharmazeutische Biologie der Friedrich-Alexander-Universität Erlangen-Nürnberg, Staudtstraße 5, D-91058 Erlangen, Germany and* [2]*Dermatologische Klinik, Krankenhaus Bethesda, Euelbuchstraße 39, D-57258 Freudenberg, Germany*

Received: 10 July 2006 Returned for revision: 12 October 2006 Accepted: 8 December 2006 Published electronically: 13 February 2007

• *Background and Aims* The floral nectary of *Digitalis purpurea* is a transitory organ with stomatal exudation of nectar. In this type of nectary, the nectar is thought to be transported to the exterior via intercellular ducts that traverse the nectariferous tissue. The latter is also traversed by a ramified system of phloem strands from which prenectar sugar is most probably unloaded. The aims of this study were to provide some of the basic information needed to evaluate the possible mechanism involved in nectar secretion and to discover the fate of the nectary.
• *Methods* The ultrastructure of the nectary was investigated at different stages of development by analysis of a series of ultrathin (7×10^{-8} m) sections 7×10^{-7} m apart from one another. Proportions of the cells typical of the nectary were documented by 3D-reconstruction and morphometry.
• *Key Results* The phloem consisted of variably shaped sieve elements and companion cells which, as a rule, were more voluminous than the sieve elements. Direct contact between the phloem strands and intercellular ducts was observed. In contrast to the phloem, which remained structurally intact beyond the secretory phase, the nectariferous tissue exhibited degenerative changes reminiscent of programmed cell death (PCD), which started as early as the onset of secretion and progressed in a cascade-like fashion until final cell death occurred in the exhausted nectary. Hallmarks of PCD were: increased vacuolation; increase in electron opacity of individual cells; progressive incorporation of plasmatic components into the vacuole reminiscent of autophagy; degradation of plastids starting with hydrolysis of starch; deformation of the nucleus and gradual disappearance of chromatin; loss of tonoplast integrity and subsequent autolysis of the rest of cellular debris. Degeneration of the cells occurred against a background of increasing cell size.
• *Conclusions* The cytological and anatomical evidence presented here, and calculations of the solute fluxes necessary for accumulation of starch and for the production of nectar support the view that: (*a*) in the foxgloves' nectary, apoplastic phloem unloading dominates, at least during exudation of nectar; (*b*) the obsolete nectary may be dismantled by PCD; and (*c*) at least the products of late nectary degradation are loaded via the apoplast into the unchanged phloem and exported to sinks elsewhere in the plant for reallocation.

Key words: Floral nectary, *Digitalis purpurea*, 3D-reconstruction, morphometry, fluid-filled intercellular space, phloem innervation, programmed cell death, nectariferous tissue.

INTRODUCTION

Although it is generally accepted that nectar originates from phloem sap (Frey-Wyssling and Agthe, 1950; Fahn, 2000), the ultrastructure of the phloem innervating nectaries has received less attention than the ultrastructure of the nectariferous tissue (secretory cells; nectary parenchyma). The sugar-secreting nectaries are undisputedly sink organs dependent on source tissue assimilates. Most of them are vascularized exclusively by phloem strands (Frei, 1955). Therefore they typify model organs for the study of unloading (release) phloem. The efflux of carbohydrates may occur across plasma membranes of the sieve element–companion cell complexes (apoplastic pathway) or through plasmodesmata interlinking these complexes with adjacent cells (symplastic pathway; Patrick *et al.*, 2001).

According to Thompson and Holbrook (2003), phloem transport depends strongly on sieve tube radius, sieve tube length and sieve plate geometry. They stressed the need for satisfactory anatomical measurements in any phloem study. The aims of the present study were (*a*) to make 3D-reconstructions and morphometry of phloem elements from series of ultrathin sections, (*b*) to look for ultrastructural criteria indicating which unloading pathway is taken in the floral nectary of *Digitalis purpurea* during nectar secretion, and (*c*) to discover the fate of the nectary after it has fulfilled its temporary function. Deletion of cells that are no longer needed is one of the functions of programmed cell death (PCD) (Pennell and Lamb, 1997; Ranganath and Nagashree, 2001). In view of the importance attached by Gray and Johal (1998) to extensive microscopic examination of the temporal sequence of subcellular events that occur during PCD, this was tried with the nectary.

MATERIALS AND METHODS

Plant material

Ovaries of *Digitalis purpurea* with nectaries at their base were collected from plants growing in a garden near Erlangen (Germany) on 1 August 1996 for investigation by transmission electron microscopy (TEM) and on 25 July 2005 for light microscopical examination. Three

* For correspondence. E-mail kgaffal@biologie.uni-erlangen.de

different stages of nectary development were chosen: (1) the onset of secretion, i.e. just before the first pair of anthers dehisced; (2) the peak period of secretion, i.e. during stigma receptivity; and (3) the cessation of secretion, i.e. after the abscission of the corolla.

Preparation and analysis

For TEM, small pieces (max. 10^{-9} m^3) of the nectaries were treated for 1 h in collidine-buffered (50 mM) 2 % glutaraldehyde containing 5 mM $CaCl_2$ at room temperature. After three 10-min rinses in collidine buffer plus 5 mM $CaCl_2$, the samples were post-fixed overnight in 2 % OsO_4 plus 0·8 % $K_3Fe_3(CN)_6$ at 4 °C. After three 10-min rinses the samples were stained *en block* for 2 h with 2 % aqueous uranyl acetate and then rinsed again three times. After standard dehydration and embedding (Spurr, 1969) a series of thin sections (7×10^{-8} m thick) were cut on a Reichert-Jung Ultracut E microtome with a diamond knife (45° Diatome, Balzers Union). From this series only every tenth section was collected and analysed. Accordingly, the distance between adjacent sections was 7×10^{-7} m.

True-to-scale models were produced either by conventional or by computer-aided 3D-reconstruction. In both cases the profiles of the structures were first traced onto transparent paper. For conventional reconstruction, the profiles were projected and traced onto polystyrene sheets of appropriate thickness. The cut-out polystyrene profiles were then well-matched and glued together. The stepped surface area was smoothed by trimming the edges of the steps and by filling the remaining corners of the steps with a paste of gypsum. After the gypsum was hard and dry the models were painted. For computer-aided 3D-reconstruction, all data processing took place using the programs ANAT3D, EDIT3D and PIC SUM (Genims International, Luxembourg) on an Atari Mega ST4 computer (Atari Corp., Sunnyvale, CA, USA). The x/y co-ordinates of the series of points placed along the profiles were digitized using a cross-hair cursor of the digitizing tablet (1st CRP Koruk, Germany). By this way the profiles of the structures were represented by polygons. The distance between adjacent profiles was 7×10^{-7} m. The reconstructions were rotated/scaled on the monitor screen until the most instructive perspective was found by eye. Stereopairs were created by rotating the reconstructed object along the vertical y-axis (3° to the left and 3° to the right). The three-dimensional details of stereopictures can be perceived by a stereoviewer or by naked-eye stereopsis. An easily learned technique for achieving unaided stereoviewing was described by McKeon and Gaffield (1990). Polychromy enhanced the discrimination of different structure elements. The same software was also used for the morphometry.

RESULTS

Ultrastructure of the nectary at the onset of secretion

A region of nectariferous tissue (NT) approx. 40–50 cells wide was located below the epidermis (Gaffal *et al.*, 1998). The latter was interspersed with permanently open stomata (Fig. 1). At the onset of secretion its cells were isodiametric and relatively small, making the nucleus appear relatively large. The cytoplasm stained homogeneously. Apart from tiny septa the intercellular spaces were devoid of structures (Fig. 2). The nuclei were more or less rotund with a smooth surface. In contrast to the more internally located nucleolus, condensed chromatin was preferentially located at the periphery, tightly attached to the nuclear envelope (Fig. 2). Several cells of the NT had a spongy appearance due to the presence of numerous smaller vacuoles that tended to be empty and to aggregate. The septa between the vacuoles differed in thickness; the thinner ones consisted of membranes only, the thicker ones were filled with cytoplasm (=plasmatic septa). Other cells had more voluminous vacuoles with inclusions that varied considerably in size, shape and structure from one another. Frequently these inclusions were membrane-bound. Occasionally irregularly shaped evaginations of the cytoplasm into the vacuoles were observed. Sporadically occurring transverse walls that were significantly thinner than mature cell walls indicated previous cell divisions. The nectariferous cells (NCs) possessed plastids (amyloplasts) containing relatively densely stained starch grains (Fig. 2). This was also the case with the epidermis including its guard cells (not shown).

Ultrastructure of the optimal secreting nectary

During secretion both the epidermal cells and the NCs differed markedly in their staining properties (Fig. 3). Consequently, the alterations of the cells were non-synchronous. This made the chronological ordering of the cytological events difficult. Although transition stages existed, the ultrastructural characteristics were classified into three categories. (1) Cytoplasm, nucleoplasm and the endomembrane system were so electron opaque that the compartmentation of the cell was hardly discernible. The existence of vesicles, for example, was indirectly indicated by their electron-transparent lumina (Fig. 3A, cells E3, E4 and N1). (2) Staining of the cytoplasm and

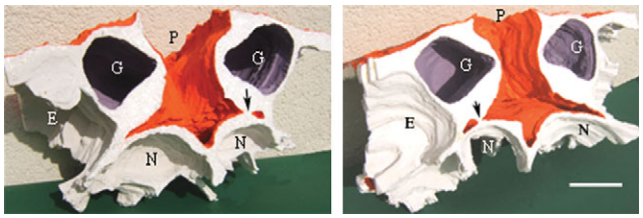

FIG. 1. Two views of a modified stomatal complex of the floral nectary of *D. purpurea*. This polystyrene model was reconstructed from 43 ultrathin sections, cut in half and painted. Surface area of epidermal cells (E), guard cells (G) and intercellular spaces (red). Surface area of the protoplast (violet). Cell walls (white). Note the narrow intercellular spaces between G and substomatal nectariferous cells (N) terminating at the stomatal pore (P). Outside these intercellular spaces the inner tangential walls of G are connected with the walls of N (arrow) thus fixing P permanently open (see also Fig. 3B). Similar connections and very small substomatal spaces were also found in several cases in the modified stomata on the floral nectary of *Vicia faba* (A. R. Davis, University of Saskatchewan, Canada, pers. comm.). Scale bar = 10^{-5} m.

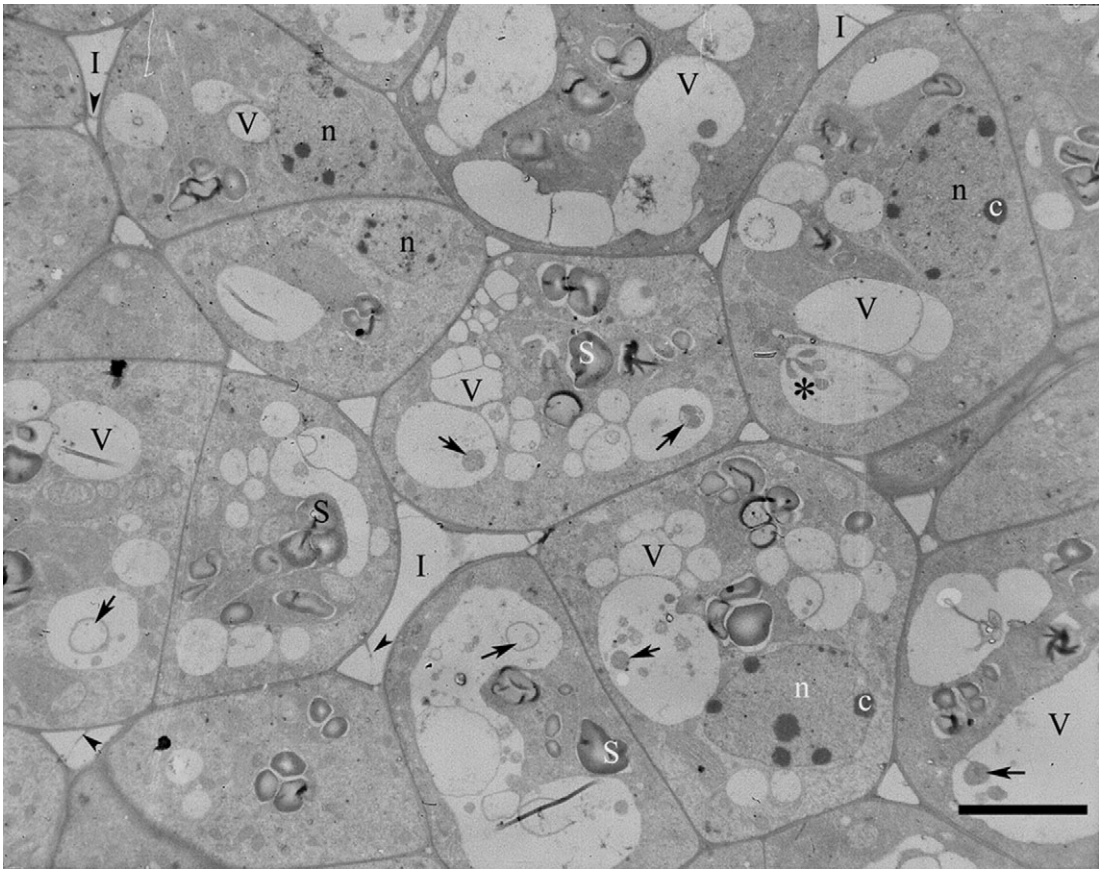

FIG. 2. Ultrastructure of the nectariferous tissue of the *D. purpurea* nectary at the onset of secretion showing similar cytoplasmic and nucleoplasmic features of the cells. The vacuome consists of variously sized vacuoles (V). In particular the more voluminous vacuoles contain multiform inclusions (arrows). Note the tiny septa (arrowheads) in the intercellular spaces (I), the plasmatic evagination into the vacuole (asterisk) and the electron opacity of chromatin (c) and starch grains (S). n, Nucleoplasm. Scale bar = 5×10^{-6} m.

nucleoplasm was moderately strong; except for vesicles, the lumina of the rest of endomembrane system were heavily stained (Fig. 3B, cells N3 and N4). (3) Staining of cytoplasm, nucleoplasm and endomembrane system was weak by way of comparison (Fig. 3B, cells N5 and N6).

Generally, more voluminous vacuoles predominated over aggregates of smaller ones. Analysis of serial sections revealed that most of the vacuoles found apparently separated in one section (Fig. 3A) were joined in adjacent sections. It was repeatedly found that only a single large vacuole existed. In addition to vacuolar inclusions resembling those found at the onset of secretion, other types of inclusions occurred: (*a*) more or less spherical structures with variably arranged electron opaque deposits (Figs 3 and 4F), (*b*) more or less dispersed electron-dense grana (Fig. 3A); (*c*) flocculent material (Fig. 4A, asterisk); (*d*) bizarre membranous structures (Fig. 3A, asterisks); and (*e*) scalloped lumps with an enigmatic internal structure that had diameters of up to 3×10^{-6} m (Figs 4Q–V).

In particular, the nuclei of the NCs tended to become flattened with a wavy outline. While the nucleoli remained unchanged, a gradual weakening of the contrast between chromatin and nucleoplasm occurred until the chromatin vanished completely. The chromatin when still visible was less often tightly attached to the nuclear envelope (Fig. 3).

The amyloplasts tended to approach the vacuole. At the sites of contact, either membrane-bound evaginations (Fig. 4A–F) or small openings [$42 \pm 20 \times 10^{-8}$ m ($\pm$ s.d.); $n = 8$] were repeatedly found. Via these openings at least the proximate starch grain appeared to be exposed to the vacuole sap (Fig. 4G–J). Generally, the starch grains were less electron dense than at the onset of secretion. In addition to the plastid-associated evaginations, which were electron translucent or filled with amorphous material (Fig. 4A–F), a great variety of other plasmatic evaginations into the vacuole were found, the larger of which were usually bounded by a double membrane (Fig. 4D, N).

In the majority of epidermal, nectariferous and companion cells, the protoplast had retracted from the cell wall leaving gaps between the wall and the plasma membrane. These gaps occurred mainly where the plasmatic coat of the vacuole was thin. They contained membranous connections between the wall and the plasma membrane (Figs. 4K–M), and/or membrane-bound vesicles (not shown), and/or irregularly shaped membrane aggregates (Figs 3 and 5A), and/or heavy deposits of electron-opaque material (Fig. 4E, F, Q–V).

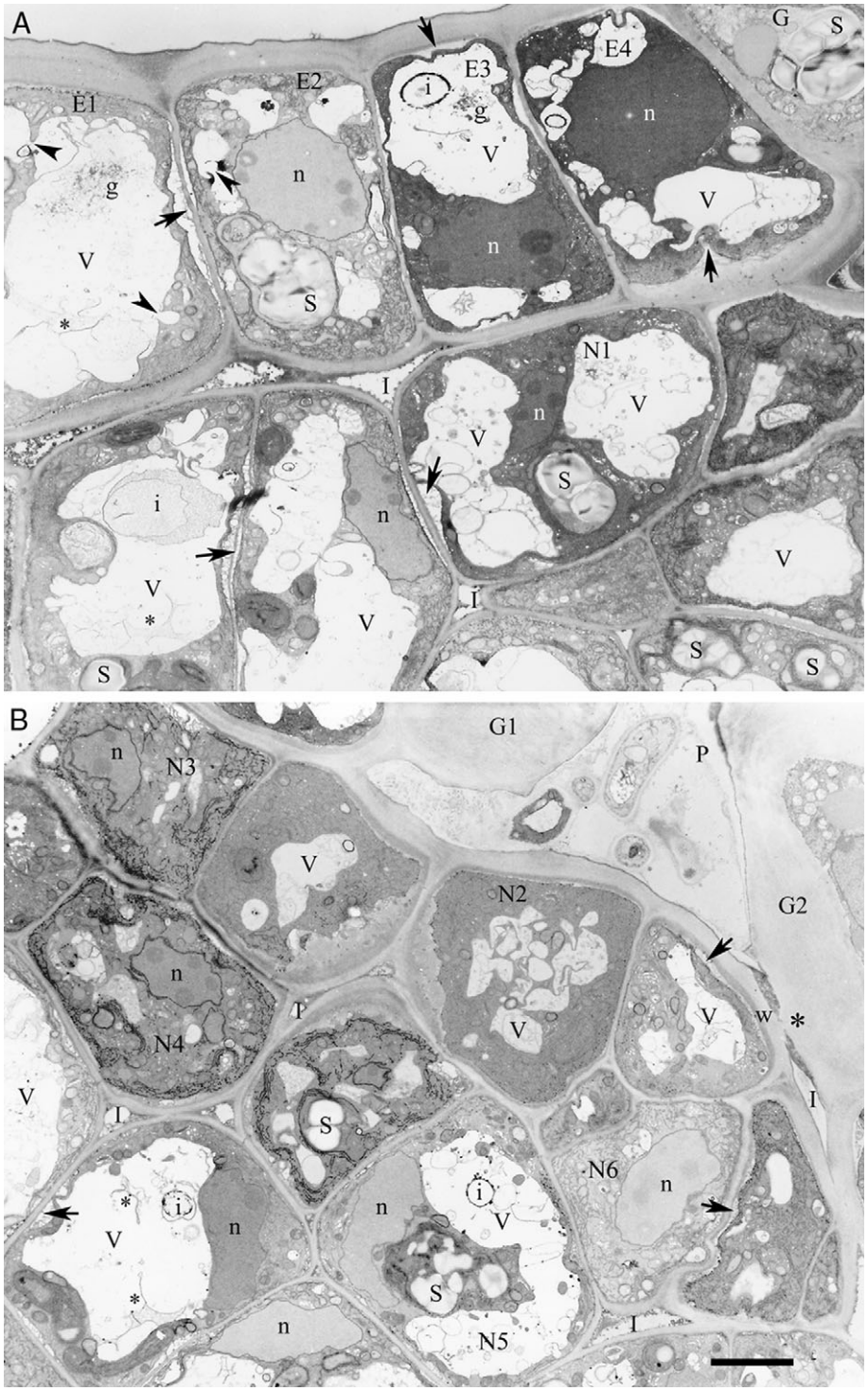

FIG. 3. Ultrastructure of the actively secreting nectary of *D. purpurea* at the periphery (A) and immediately below (B) a stoma showing the variety of cytological features in both the epidermal (E) and nectariferous (N) cells. Note multivarious inclusions (i) and electron-dense grana (g) in the vacuome (V) and occasional separation of the protoplasts from the cell walls (arrows). Most of the plastids of G (guard cell), E and N contain starch (S). Intercellular spaces (I) are covered with granules. n, Nucleoplasm. In (A) note the obviously opened septa between adjacent vacuolar spaces (arrowheads) in E1 and E2, two of which are relatively thick (=plasmatic septa). The electron opacity of the remains of the septum in E2 and the deposit attached to the septum in E1 suggest steps of plasmatic septum degeneration. Serial sections proved that the two vacuolar spaces seen in N1 belong to a single vacuole. In (B) the ventral wall of G2 (asterisk) is connected with the wall (w) of a substomatal N thus fixing the stoma permanently open. In N2 the vacuolar compartments are still separated from one another by irregularly shaped protoplasmic septa. Note the microbes inside the stomatal orifice (P). Scale bar = 5×10^{-6} m.

The vascular supply entering the NT consisted of reticulating phloem strands that terminated approx. 8–12 cell layers below the epidermis (Gaffal *et al.*, 1998). Most probably it is here that unloading occurs. Diagnostic features of the sieve elements (SEs) are either the sieve plates by which they are joined to each other or peculiar plastids (Behnke, 1991), which in this case are of the SS-type (Fig. 5A, E).

At the magnification usually used in the examination of the secreting nectary, it was very difficult to identify with certainty the cells adjacent to the SEs. Two types of cells were present: those that were similar in internal structure to NCs and those that usually displayed maximum staining of the cytoplasm and lacked starch grains. The latter proved to be companion cells (CCs) not only by the absence of starch but also by being linked with their SEs via pore–plasmodesma complexes (Fig. 5E). There were relatively few plasmodesmata connecting the sieve element–companion cell–complexes (SE-CC-Cs) to surrounding cells; i.e. the phloem was somewhat isolated symplastically.

Intercellular spaces were not only found between the epidermal cells (inclusive guard cells) and the NT, and between the NCs (Figs 1 and 3) but they also abutted the phloem strands (Figs 5A, E, 6 and 8A). These contacts support the view that the phloem termini lack typical bundle sheath cells. Most of the intercellular spaces contained small electron-opaque particles (Figs 3 and 4Q–V) that were similar to those particles found at the periphery of the protoplast of several cells (Fig. 4K–M), and in some of the gaps between the cell wall and the plasma membrane (Fig. 4F, Q–V).

Ultrastructure of the exhausted nectary

After cessation of nectar exudation, heterogeneity in cellular features of the NT still existed. The epidermal cells (exclusive of guard cells) and the NT were devoid of plastids, indicating that not only the starch but also other components of the plastids had been hydrolysed during the secretory stage. The NCs, now appearing more or less empty, varied greatly in volume ($1330 - 4480 \times 10^{-9}\ m^3$), shape and contents from one another. The mean value ($2250 \pm 1140 \times 10^{-9}\ m^3$, $n = 6$) was almost double that of the NCs in the active nectary ($1199 \pm 319 \times 10^{-9}\ m^3$, Gaffal *et al.*, 1998). Frequently the interfaces of neighbouring NCs undulated (Fig. 5E). Analysis of serial sections revealed that such cells, by lacking a nucleus and a structurally intact cytoplasm, were nothing more than cell corpses. Their lumina contained variable aggregates of granules and lipid-like globules, which were obviously connected by remnants of the plasmalemma (Fig. 5B–E). However, some NCs still contained a nucleus and a few mitochondria, with a single central vacuole occupying most of their volume and with the cytoplasm being confined to a narrow peripheral layer surrounding the vacuole. Gaps between the cell wall and plasma membrane were no longer found (Fig. 5B). The cytoplasm contained lipid-like globules that were devoid of internal structure and did not appear to be membrane-bound. Although they tended to distend the tonoplast they were not pinched off into the vacuole (Fig. 5B, C), but remained attached to cytoplasmic remnants until very late in cytoplasmic degeneration. Cytoplasmic collapse was preceded by loss of the tonoplast, detachment of the plasma membrane from the cell wall and spread of the vacuolar sap across the whole cell lumen (Fig. 5D). Mitochondria and the usually flattened nucleus seemed to be degraded along with or immediately after the tonoplast. The majority of intercellular spaces were again devoid of internal structures. Occasionally, however, lipid-like globules were found (Fig. 5B).

In contrast to the NT, the phloem innervation remained almost unchanged. Therefore, the CCs still rich in mitochondria could be easily identified (Fig. 5B, E). It could be shown that there was, on average, one CC for each SE. Ultrastructural differences between the SE-CC-Cs of the active and the exhausted nectary are restricted to an apparent numerical increase of vacuolar inclusions in the CCs of the exhausted nectary. The SEs, however, displayed an identical ultrastructure. The sieve plate pore diameter was $40 \pm 4 \times 10^{-8}$ m ($n = 19$) in the active nectary and $41 \pm 5 \times 10^{-8}$ m ($n = 29$) in the exhausted nectary with a plate thickness of $56 \pm 6 \times 10^{-8}$ m ($n = 16$) and $58 \pm 7 \times 10^{-8}$ m ($n = 18$), respectively, and the total pore area was approx. 50 % of the plate area. The pores appeared to be filled with two differently stained components: an electron-translucent callose collar surrounded a darkly stained and irregularly shaped core (Fig. 5A, E). The SEs not only displayed various shapes but they also did not form straight files, i.e. a zigzag path of sieve tubes existed (Figs 6 and 8B). The SEs differed from one another by the number of interfaces that they shared with other SEs. Terminal SEs were connected by only one sieve plate with subterminal SEs, whereas the latter and other interstitial SEs shared at least two sieve plates with their neighbours. Individual SEs were shown to be in contact with up to five other SEs (Fig. 7A).

The intercellular contact between SEs and other types of neighbouring cells was also variable. As a rule, SEs were in contact with more than one CC (Fig. 7B). These interfaces, however, differed markedly in size. The largest interface indisputably resulted from division of the mother cell into the SE-CC sisters. These sisters sometimes had almost equal volumes, but on average CCs were more voluminous ($V = 650 \pm 134 \times 10^{-9}\ m^3$; $n = 6$; range: $489–809 \times 10^{-9}\ m^3$) than SEs ($V = 489 \pm 103 \times 10^{-9}\ m^3$; $n = 5$; range: $384 - 603 \times 10^{-9}\ m^3$). Whereas SEs inside the phloem strands lacked contact both with NCs and with intercellular spaces, peripheral and, in particular, terminal SEs shared up to 68 % of their surface area with NCs, and up to 6 % with intercellular spaces (Fig. 9).

The fate of the post-secretory nectary

Light-microscopical examination of hand sections through fresh ovaries revealed that (*a*) the diameter of the active nectary increased by approx. 25 % during secretion, (*b*) while the maximum diameter of the ovary increased about 2-fold, the peripheral diameter of the exhausted nectary increased only slightly by about 10–20 % after

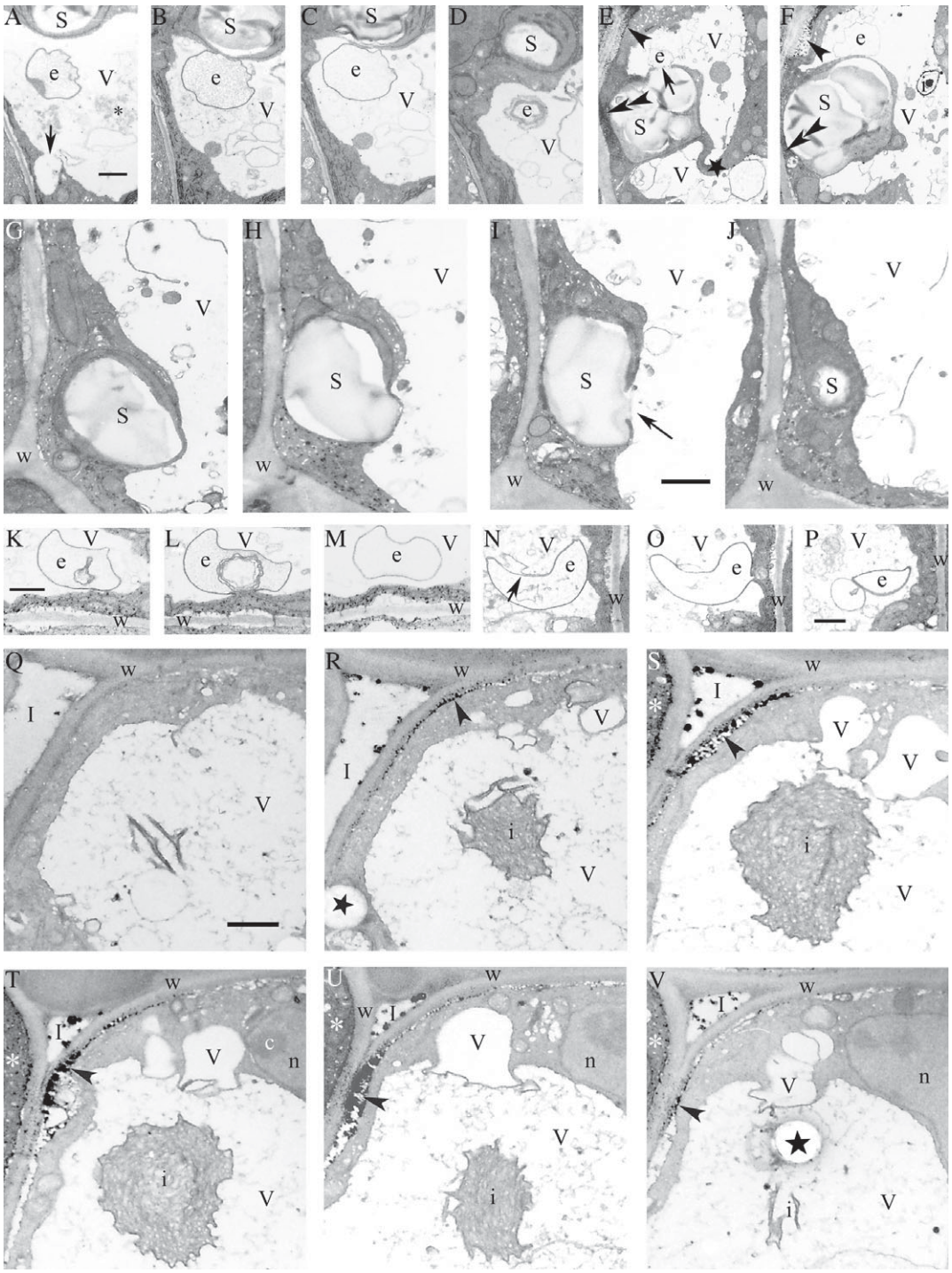

FIG. 4. Series of sections through plastid-associated membranous evaginations (e) into the vacuole (V) (A–D, E, F), plastid-associated opening into V (G–J), other types of membranous evaginations into V (K–M, N–P), and a relatively voluminous vacuolar inclusion (i) (Q–V), indicating that the incorporation of structured or structureless cytoplasmic components into V may occur by pinching off of smaller portions (A–F, K–P), via leaks (G–J) and by segmentation of larger portions (Q–V). (A) Note rupture of the septum between a small V and the central V (arrow). (D) The grazing section through e documents that the envelope of e is a double membrane. (E, F) The plasmatic septum between the two spaces of V (star in E) is lacking in (F). Loss of dense material at the periphery of the plastid (arrow) seems to be correlated with the formation of e. Note the electron opaque particles at the periphery of the protoplast (double arrowhead), in the space between the protoplast and the cell wall (arrowhead in F), and the vacuolar inclusion (i) with electron-opaque deposits. (I) Note the open access of the vacuole sap to the starch (S) grain (arrow). (N) Note the envelope of e is split into two membranes (arrow). (Q–V) In contrast to the left cell, the cytoplasm of which is visible only from S–V (white asterisks), the cytoplasm of the right cell lacks electron-opaque structures. Note heavy deposits of electron-opaque material in the space between the plasmatic coat of V and the cell wall (w) in the right cell (arrowheads) and in the intercellular space (I). Formation of a single vacuole is not yet finished. The vacuole-like areas (stars) are artefacts caused by holes in the supporting film of the sections. Scale bars = 10^{-6} m.

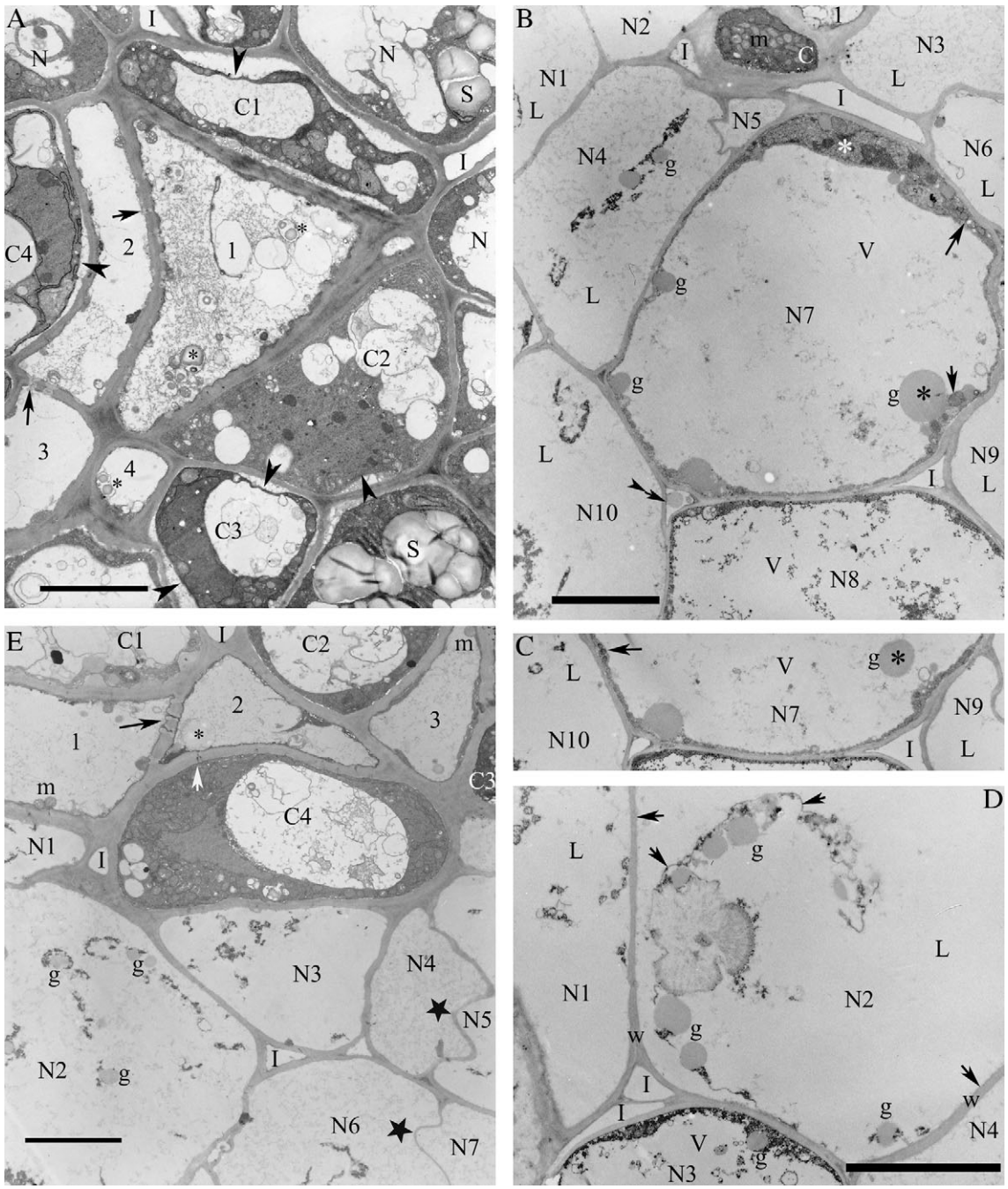

FIG. 5. Ultrastructure of the phloem and adjacent nectariferous cells in the actively secreting (A) and in the exhausted nectary (B–E) of *D. purpurea*. Whereas the sieve elements (labelled with numbers) and companion cells (C1–C4) retained most of their structural identity in both developmental stages (A, B, E), the nectariferous cells (N) differ markedly in structure from one another. (A) Note the sieve element-specific plastids (asterisks), sieve pores (arrows), intercellular spaces (I) abutting C1, and detachment of C protoplasts from cell walls (arrowheads). Companion cells are devoid of starch grains (S). Degradation of N resembles that seen in Fig. 3. (B) Among a total of ten cells (N1–N10), two (N7 and N8) are still equipped with a thin peripheral plasmatic coat of the enlarged vacuole (V). Lipid-like globules (g) adhere not only to the plasmatic coat, but also to plasmatic debris freely scattered in the lumen (L) of N4 and N10. Note the high density of mitochondria (m) in C indicating the large energy need of companion cells, the extremely flattened nucleus (white asterisk in N7), a lipid-like globule in intercellular space (double arrowhead) and several other cytoplasmic compartments-most probably mitochondria (arrows in N7). (C) Serial section adjacent to that seen in (B). The globule (asterisk) appears to be isolated, but is not, as seen in (B). (D) N3 still retains a plasmatic coat of V. N2 contains a portion of cytoplasmic debris that obviously originated from rupture and retraction of the original plasmatic coat from the cell wall (w). As a result the outside of the plasma membrane and the inside of w come into contact (arrows) with the vacuolar sap that fills the whole cell lumen (L). (E) The nectariferous cells seen here are in the last phase of degradation, which is characterized by erosion of the vestiges of cytoplasm. Buckling of cell walls occurs along with advanced disintegration (stars). Note the structural integrity of the sieve elements 1–3 with sieve element-specific plastids (asterisk), sieve pores (arrow), mitochondria (m) and the pore-plasmodesmata complex between 2 and C4, which is typically branched towards C4 (white arrow). Intercellular spaces are not only interspersed among the nectariferous cells, but also abut 2 and C4. Scale bars = 5×10^{-6} m.

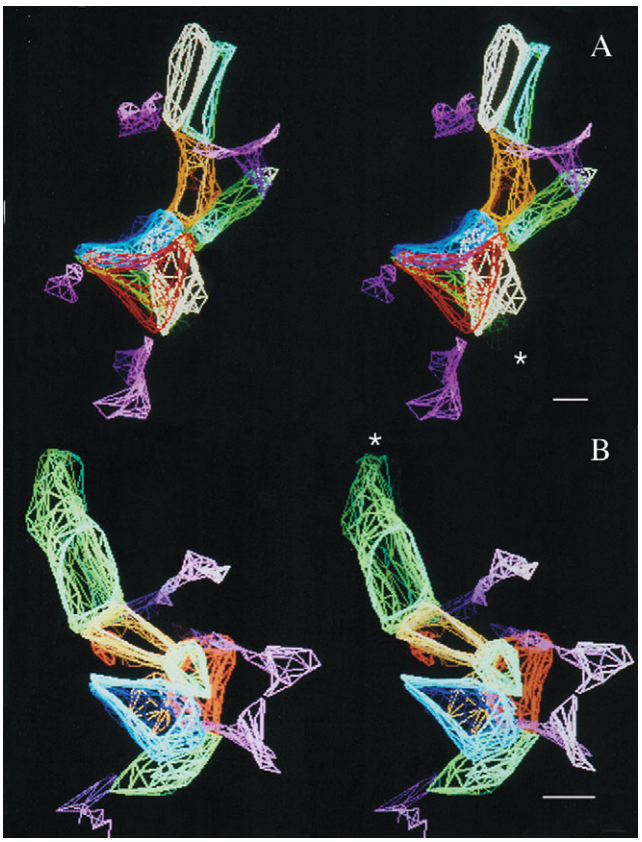

FIG. 6. Stereopairs of computer-aided reconstructions of those parts of a total of 17 sieve elements incorporated in a $9{\cdot}1 \times 10^{-6}$ m thick slice of an actively secreting nectary of *D. purpurea*. The asterisks indicate where the two models are connected with one another. Only those ends of the intercellular reticulum (violet) adjoining sieve elements are reconstructed. In (A) both the white (below the centre) and the brown, and in (B) the red (below the centre) sieve elements are in contact with five other sieve elements. For ultrastructure of the red, blue, brown and green (on the right) sieve elements in (A) see 1–4 in Fig. 5A. Scale bars = approx. 5×10^{-6} m.

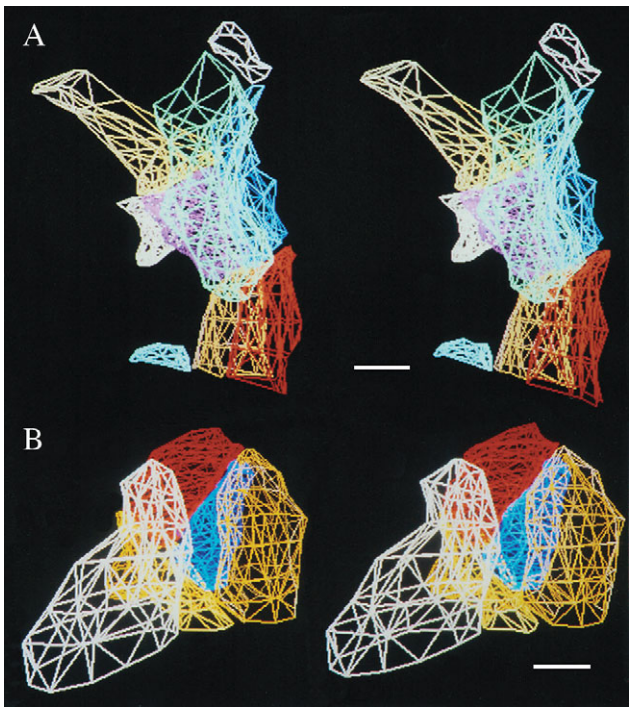

FIG. 7. Stereopairs of computer-aided reconstructions of a sieve element (violet in A, blue in B) that is in contact with five other sieve elements (A) and four companion cells (B). The models, viewed from different sides, are based on a $23{\cdot}8 \times 10^{-6}$ m (A) and a $18{\cdot}9 \times 10^{-6}$ m (B) thick slice of an exhausted nectary of *D. purpurea*. For the morphometry of the interfaces of this sieve element, see Fig. 9A. Scale bars = 5×10^{-6} m.

cessation of secretion, and (*c*) while the horziontal height of the corpse of the nectary bulge did not change markedly, the vertical width was reduced significantly to about 30 % of that in the active nectary (Table 1). The basal nectary bulge became inconspicuous and a brownish stained layer of crushed cell corpses remained.

DISCUSSION

Sink to source transition

According to the classification of sinks into the categories (i) consuming, (ii) accumulating, (iii) secreting (Zamski, 1996), the nectary of *D. purpurea* changes from both a consuming and accumulating body during growth and starch deposition to a secreting one. During secretion the nectary is not only a sink but it also becomes a source, because a number of hallmark features that indicated the onset of PCD were observed (see 'Hallmarks of PCD'). Nutrient element mobilization and recycling in surviving parts of the plant are central features of PCD (Rubinstein, 2000; Huelskamp and Schnittinger, 2004). There is reason to believe the SEs and CCs remain functional until very late, perhaps dying only after the surrounding NCs have collapsed. The surviving phloem appears to be involved in the uptake and export of products of cellular catabolism from the dying nectary to sinks elsewhere in the plant. In addition to senescing leaves and corollas (Matile and Winkenbach, 1971; Noodén and Leopold, 1988; Bieleski, 1995), the nectary is another example of the marked persistence of phloem activity in a background of dying cells and the rapid reversal in sink–source behaviour.

Solute flux necessary for nectar production

The nectar of *D. purpurea* was composed of 78·4 % sucrose, 10·5 % glucose and 11·1 % fructose (Lichius *et al.*, 1990). On average, the daily amount of nectar produced by one flower of *D. purpurea* was 11·6 mg containing 16–27 % sugar (Percival and Morgan, 1965), 13·7 mg containing 24–45 % sugar (Halmágyi and Gulyás, 1970), and 11·1 mg containing 23·6 % sugar (Assmann, 1986). This is equivalent to about 470 − 1300 mM sucrose. The lower concentration resulted from daily exploitation, thus indicating that the sugar concentration of nascent nectar was near this value. In nectar that is exposed to the environment for longer times, sugars accumulate to

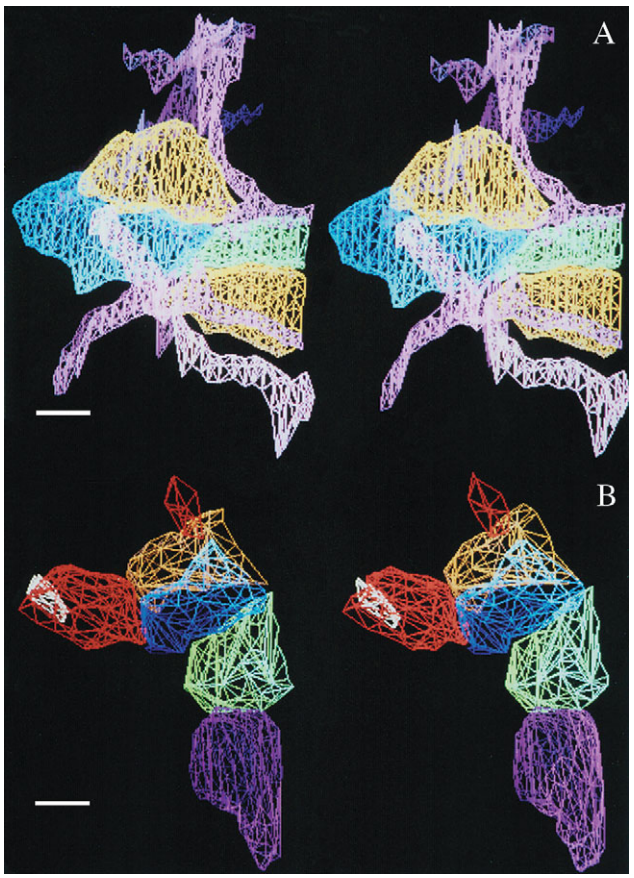

FIG. 8. Stereopairs of computer-aided reconstructions of two tips of the ramifying phloem innervation incorporated in a $23{\cdot}8 \times 10^{-6}$ m thick slice of an exhausted nectary of *D. purpurea.* (A) exhibits a terminal (blue) and a portion of a subterminal (green) sieve element, companion cells (yellow) associated with the terminal and subterminal sieve elements, and the intercellular reticulum (violet) abutting upon these phloem elements. For the morphometry of the interfaces of the terminal sieve element and its companion cell, see Fig. 9C and K. (B) exhibits a complete terminal sieve element (violet) and portions of the six adjoining sieve elements. Both tapering (yellow, blue, red) and furcation (blue, green) of the sieve tubes are documented. For the morphometry of the interfaces of the club-shaped terminal sieve element (violet), see Fig. 9E. Scale bars = 5×10^{-6} m.

higher concentrations due to evaporation of water. In the phloem sap, sugar (in most species almost exclusively sucrose) also reached very high levels, usually ranging from 200 to 1600 mM (Winter and Huber, 2000). Assuming that (*a*) sugar concentration in nascent nectar is 440 mM, one flower may secrete $15–30 \times 10^{-9}$ m^3 nectar a day, (*b*) the nascent nectar and the phloem sap coincide in sucrose concentration, and (*c*) that only the 78·4% share of sucrose in the nectar originates from the phloem sap, then approx. $118–236 \times 10^{-10}$ m^3 phloem sap has to be translocated per day via the phloem vasculature of the nectary. The volume of the nectary is approx. 2×10^{-9} m^3 (Gaffal *et al.*, 1998), but only a small fraction is allotted to the sieve tubes. Estimating 1%, then nectar secretion loads new sap to the extent that the entire volume of the sieve tubes must be refilled 590–1180 times per day.

Solute flux necessary for starch production

In order to get an idea of the sucrose flux necessary for storage of starch, it was estimated that at the onset of nectar secretion, 10–20 % of the volume of the nectary (about 2×10^{-9} m^3) of *D. purpurea* is occupied by starch, i.e. a maximum of 4×10^{-10} m^3. By taking a median density of starch (1·34 mg mm^{-3}), it is converted to a maximum of 0·54 mg starch. Because the amount of energy per mass of starch (4·15 kcal g^{-1} from maize) and of sucrose (4·1 kcal g^{-1}) are almost equivalent to one another (Neumüller, 1979), it can be roughly estimated that 0·54 mg starch originates from about 0·54 mg of sucrose. In this balance of energy the expenditure of energy for the synthesis of starch from sucrose is not taken into consideration. Therefore this value is underestimated to an unknown degree. However, the error is reduced because the calculation is with the upper limit of starch content. Because $3{\cdot}6 \times 10^{-9}$ m^3 of a 15 % solution contain 0·54 mg sucrose, the phloem vasculature of the nectary (2×10^{-11} m^3) has to be refilled 180 times. It appears that, similar to starch accumulation in other nectaries (Razem and Davis, 1999; Peng *et al.*, 2004), it takes >1 d to deposit the starch. But even if this 1-d interval is used, the rate of sucrose flux during the accumulation of starch would be at least three to seven times smaller than during the secretion of nectar. Hence, the sink strength of the nectary seems to increase during secretion. The temporarily enhanced sucrose unloading capacity may result either from intensification of the unloading system or from turning on a specific efflux mechanism.

Origin of nectar

The coincidence of nectar secretion and degradation of starch in the NT has been a well-known phenomenon for more than a century (Behrens, 1879). Recently, *NEC1*, a gene predominantly expressed in the nectaries of *Petunia hybrida*, was cloned (Ge *et al.*, 2000). The pattern of *NEC1* expression appeared to follow the temporal events of starch hydrolysis, thus supporting the hypothesis that *NEC1* is involved in the process of nectar secretion. However, as early as 1886, Stadler questioned the origin of nectar in nectaries that lacked adequate quantities of starch (Stadler, 1886). He, and more recently Horner *et al.* (2003), suggested that such nectaries, after being fed with fluid nectar-producing precursors from sources elsewhere in the plant, might secrete it directly without an intermediate storage form of reserves. The calculations above suggest that sugar originating from starch degradation plays only a minor role in nectar production of *D. purpurea*. The bulk of nectar seems to be directly unloaded from the phloem sap. The decrease in nectar production after reduction of the assimilate transport by girdling flowering shoots (von Czarnowski, 1952; Wykes, 1952) or by darkening and defoliation experiments (von Czarnowski, 1952; Pleasants and Chaplin, 1983; Nepi *et al.*, 2005) strongly favours the view that a good deal of nectar is supplied from the current assimilate flux.

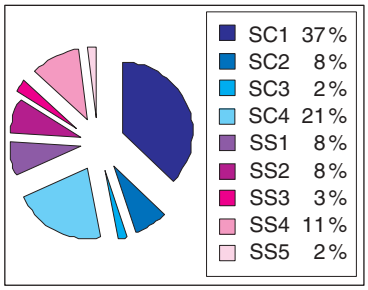

(A) Surface area of S: approx. $3{\cdot}1 \times 10^{-10}$ m^2

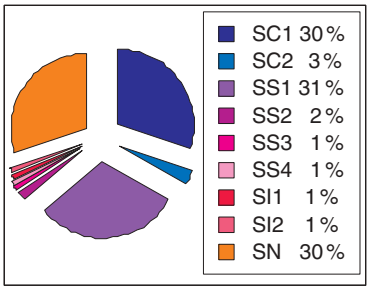

(B) Surface area of S: approx. $4{\cdot}7 \times 10^{-10}$ m^2

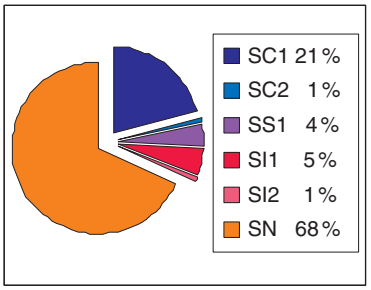

(C) Surface area of S: approx. $3{\cdot}4 \times 10^{-10}$ m^2

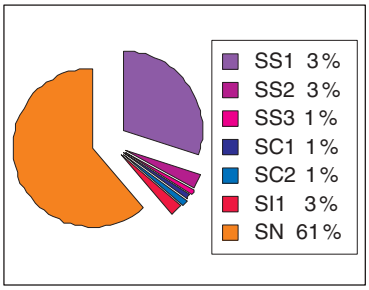

(D) Surface area of S: approx. $4{\cdot}9 \times 10^{-10}$ m^2

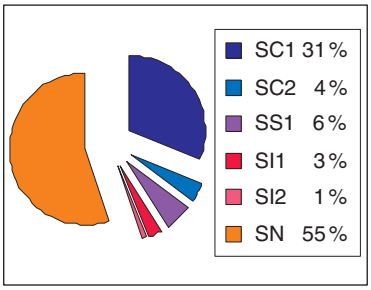

(E) Surface area of S: approx. $2{\cdot}6 \times 10^{-10}$ m^2

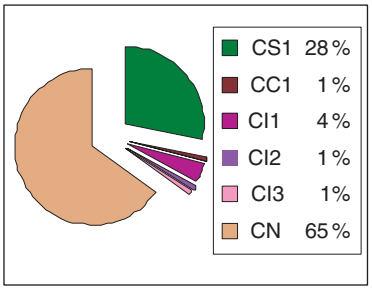

(F) Surface area of C: approx. 5×10^{-10} m^2

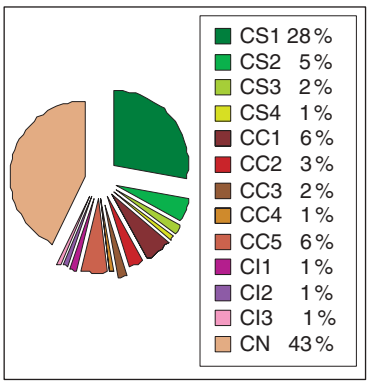

(G) Surface area of C: approx. $4{\cdot}3 \times 10^{-10}$ m^2

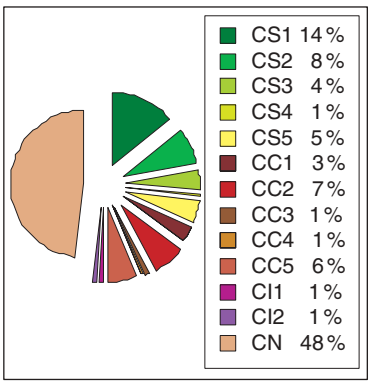

(H) Surface area of C: approx. $4{\cdot}4 \times 10^{-10}$ m^2

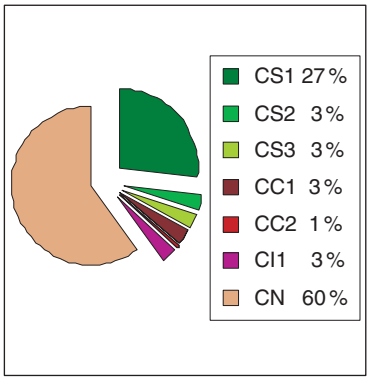

(I) Surface area of C: approx. $3{\cdot}8 \times 10^{-10}$ m^2

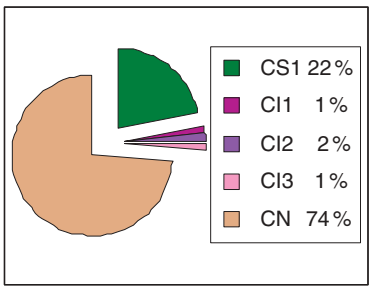

(J) Surface area of C: approx. $3{\cdot}3 \times 10^{-10}$ m^2

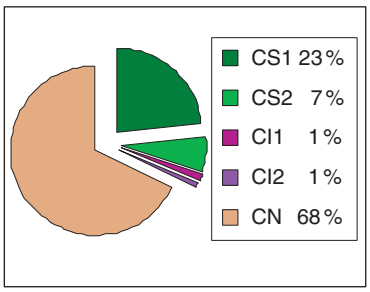

(K) Surface area of C: approx. $3{\cdot}5 \times 10^{-10}$ m^2

FIG. 9. Interfaces between individual sieve elements S ($n = 5$; A–E) or companion cells C ($n = 6$; F–K) and adjacent structures (a) adjacent cells (other sieve elements S1–Sn, other companion cells C1–Cn, nectariferous tissue N) and (b) intercellular spaces I1–In, expressed in percentage terms.

TABLE 1. *Data (m^{-3}) from median sections of the ovary of* D. purpurea*: on its maximum diameter (A), on the peripheral diameter of the nectary or its remains (B), on the height (Ch) and the basal width (Cw) of the upper nectary bulge or its remains, on the height (Dh) and basal width (Dw) of the lower bulge or its remains, at the onset of nectar secretion (1), during secretion (2), at cessation of secretion (3), during progress in growth and ripening of the fruit (4–9)*

	A	B	Ch	Cw	Ch : Cw*	Dh	Dw	Dh : Dw*
1	4	4	0·27	0·54	0·5	0·25	0·5	0·5
2	4·5	4·5	0·18	0·46	0·39	0·25	0·5	0·5
3	5·5	5	–	–	–	0·43	0·57	0·75
4	6·5	4·5	0·32	0·36	0·89	0·36	0·43	0·84
5	7	6	0·25	0·21	1·19	–	–	–
6	11	5	0·25	0·18	1·39	0·29	0·36	0·81
7	11	6	0·21	0·25	0·84	0·29	0·21	1·38
8	10·5	6	0·29	0·16	1·81	0·29	0·18	1·61
9	10	5·5	0·25	0·14	1·78	0·25	0·14	1·78

* The increase of the h : w ratio results mainly from reduction of the basal width of the nectary bulge.

Morphotype of the nectary phloem

Morphometry established that the CCs of the phloem strands innervating the floral nectaries of *D. purpurea* and *Isoplexis canariensis* (Gaffal and El-Gammal, 2003) are typically more voluminous than the SEs. A similar ratio in size is not only evident from studies on other nectaries (fig. 3 in Figier, 1971; Findlay and Mercer, 1971; Durkee *et al.*, 1981; Durkee, 1983; Davis *et al.*, 1986, 1988; Razem and Davis, 1999; fig. 3 in Zhu and Hu, 2002; Wist and Davis, 2006) but also from studies on the vasculature of other sink tissues. CCs at least as wide as the SEs were found in the unloading phloem of the rice pericarp (Oparka and Gates, 1981), in the minor bundle of the developing apple fruit (fig. 7a, c in Peng *et al.*, 2003), and in the phloem feeding the pericarp and the cotyledons (named 'seed pericarp') of developing walnut fruit (fig. 2 in Wu *et al.*, 2004). The large size of the CCs relative to the SEs in special regions of phloem unloading is the reverse of that found in the transport phloem, but quite similar to that of leaf minor veins (for instance, Haritatos *et al.*, 2000), where phloem loading occurs. The large size of the CCs is thought to reflect their active role not only in phloem loading (Barth *et al.*, 2003), but also in the unloading process (Oparka and Gates, 1981; Findlay, 1988).

Ramification of the phloem innervation causing bifurcation of the solute flux necessitates at least tripolar SEs. Multipolar (more than tripolar) SEs are junctions where solute inflow from more than one SE and solute outflow into more than one SE can meet. The amount of inflow from and outflow into adjacent SEs seems to depend on the number of sieve pores per interface. Solute distribution may be controlled in this way. Multipolar SEs interlinked via sieve plates with more than two SEs are known from leaf veins (Koch, 1884) and from wound phloem (Eschrich, 1953, Schulz, 1986). The sieve tubes of the latter, obviously an unloading phloem, are zigzag shaped, similar to those of the nectary phloem. Between two given points a straight sieve tube is not only shorter than a zigzag-shaped one, but will also exert less frictional resistance to the solute flux. If future studies corroborate that such anatomical features are typical of unloading phloem, models of solute flux should incorporate the effects introduced by shape.

Open access of phloem to intercellular space

Phloem elements in contact with intercellular spaces were found not only in this and more recent studies on nectaries of (*a*) *Helianthus annuus* var. *macrocarpus* (fig. 5 in Sammataro *et al.*, 1985); (*b*) *Vicia faba* (Davis *et al.*, 1988); (*c*) *Pisum sativum* (Razem and Davis, 1999); (*d*) *Isoplexis canariensis* (Gaffal and El-Gammal, 2003); (*e*) *Echinacea purpurea* (Wist and Davis, 2006), but also more than a century ago. Intercellular ducts abutting the vasculature of the nectary of *Serratula lycophila* were interpreted to be involved in the secretion of nectar (von Wettstein, 1889). In the nectaries of Paeoniaceae (Zimmermann, 1932; Frey-Wyssling and Häusermann, 1960; Hiepko, 1966) cells of the so-called 'conducting tissue' [Leitparenchym (obviously phloem elements)] even adjoined the substomatal spaces of those 'stomata' (Discusspalten) through which the nectar escaped to the outside. This structural specialization, which most probably also exists in *Helianthus* (fig. 5 in Sammataro *et al.*, 1985), indicated the possibility of a direct unloading of assimilates from the phloem to the exterior of the plant (Zimmermann, 1932; Hiepko, 1966; Schnepf, 1973), and might also explain why exclusively sucrose was found in the nectar of *Paeonia* (Frey-Wyssling and Häusermann, 1960). A sucrose-dominant nectar is also secreted from the petal tip of *Medinilla magnifica* (Tobe *et al.*, 1989). There any NT (nectary parenchyma) is missing, but the associated vascular bundle consisting of phloem only is thickened. This anatomical evidence again indicates that the nectary is the phloem-rich median petal bundle itself. Although it remains to be proven that the reticulum of intercellular spaces terminating at the permanently open stomata of the nectary (Gaffal *et al.*, 1998) is connected with the reticulum of intercellular spaces arriving at the phloem strands, there is a good chance for the existence of continuity. Two fundamental differences exist between the nectaries of *Paeonia* and *Medinilla* on the one hand, and *D. purpurea* on the other hand. (1) The length of the path the nectar has to pass through the intercellular space of the NT until it is discharged to the surface of the nectary via the modified stomata is much longer in the nectary of *D. purpurea.* The chemical composition of the nectar may be altered along this passage. For instance, invertases located in the cell wall boundary of the intercellular spaces may form glucose and fructose from the raw material of the nascent nectar (sucrose). (2) Starch in the nectary parenchyma is hydrolysed during secretion, and sugars originating from this decomposition may enter the intercellular spaces and influence the chemical composition of the nectar.

Intercellular spaces that abut against phloem elements are not limited to nectaries. They were clearly seen (*a*) between

unloading phloem cells of the developing apple fruit (fig. 7a, c in Peng *et al.*, 2003), (*b*) in minor veins of developing tobacco leaves (fig. 4 in Wright *et al.*, 2003), (*c*) in minor veins of the leaves of transgenic potato plants (figs 18 and 19 in Schulz *et al.*, 1998) and (*d*) in adaxial minor veins of *Cucurbita pepo* leaves (fig. 3 in Turgeon and Webb, 1976), which were suggested to constitute the preferential pathway for the import of assimilates.

The apoplast of the secreting nectary

During secretion the intercellular space of the nectary is most probably filled with nascent nectar. Positive staining for carbohydrates indicated their presence in the intercellular spaces of the extrafloral nectaries of Australian acacias (Marginson *et al.*, 1985). Because the prenectar has to pass the cell wall, we think that the sugar concentrations of the fluid in the wall apoplast and in the intercellular space are identical. Accordingly, the sink end of the phloem pathway may be surrounded by an apoplast solution with a concentration of osmotically active solutes not drastically different from that of the phloem sap. Therefore, unloading of sucrose from the phloem pathway that is driven by large transmembrane concentration differences seems to play a minor role. High sucrose concentration in the cell wall apoplast favours an energy-dependent and possibly carrier-mediated process as postulated for strong sinks (Wolswinkel, 1985), such as ripening grape berries (Wang *et al.*, 2003). In theory, the unloading of sucrose into the apoplast could occur by specific effluxers that either use a proton antiport mechanism or are directly energized by ATP (Lalonde *et al.*, 2004). ATP-ase activity was detected by cytochemistry in the phloem tissue adjacent to the nectaries of *Gossypium* (Eleftheriou and Hall, 1983) and *Hibiscus* (Sawidis, 1991).

The mechanisms of nectar secretion proposed by Vassilyev (2003) and Koteyeva *et al.* (2005) were based on the idea that the apoplast of the NT forms the main route taken by the nectar sugars on their way to the stomatal opening. Although the actual direction faced by the wall ingrowths of the nectary CCs (which are transfer cells) of *Vicia faba* (Davis *et al.*, 1988) clearly suggested an avenue for unloading of pre-nectar constituents directly to intercellular spaces (i.e. apoplast), Vassilyev (2003) and Koteyeva *et al.* (2005) either ignored the CCs of the nectary phloem or assigned them only a passive role in assimilate transport. Except for the substomatal cavity, Vassilyev's fig. 1 also lacked intercellular spaces. In contradiction to this model, the sites of open access of the SE-CC-Cs to the intercellular system were considered to be the shortest pathways for an apoplastic efflux of assimilates (Gaffal and Heimler, 2000).

Hallmarks of PCD

During secretion and the final degradation phase of the nectary, a number of hallmark features arise that are reminescent of autophagy and autolysis. These symptoms are common in plants and appeared during normal pericarp development and may therefore indicate developmental PCD (Dangl *et al.*, 2000; van Doorn and Woltering, 2005). The phenotype of PCD in the foxglove's nectary is definitively very similar to that in the nectary of *Glycine max* (Horner *et al.*, 2003), and to the phenotype of senescence in the petals of *Ipomoea* (Matile and Winkenbach, 1971), *Dianthus* (Smith *et al.*, 1992) and *Hemerocallis* (Stead and van Doorn, 1994). Senescence is considered to be a type of PCD (Noodén, 2004). The sequence of cell degeneration discussed here is an interpretation without independent confirmation that one stage neccessarily leads to another.

(a) Increased vacuolation. One of the earliest events observed is the fusion of smaller vacuoles, which culminates in the formation of a single central vacuole. This obviously occurs by rupture or degradation of the tonoplast-coated septa between adjacent vacuolar spaces (Figs 3A and 4A, E, F). Some of the vacuolar inclusions seem to originate from these events. Further enlargement of the central vacuole is associated with the extension growth of the dying but still expanding NCs. The NCs of *Eccremocarpus scaber* also increased 2-fold in volume during their development (Belmonte *et al.*, 1994). Significant changes in the vacuome, usually in the form of increased vacuolation, were widely reported in plant PCD (Rogers, 2005).

(b) Autophagy. Vacuolar inclusions also seem to originate from the pinching off of plasmatic evaginations into the vacuole. With progression through the PCD process, incorporation of plasmatic components into the vacuole increases in number. Degradation of vacuolar inclusions seems to occur through autophagy. In dying plant cells there is ample evidence for vacuolar autophagy (Krishnamurthy *et al.*, 2000). Autophagic PCD is normally used for recycling cellular components (Lam, 2004), since progressive elimination of cytoplasm by hydrolysis in vacuoles extends the survival of the dying cell and efficient withdrawal of nutrients from the cells can be achieved (Jones, 2000; Mittler and Cheung, 2004).

(c) Degradation of plastids. The decrease in electron opacity of the starch grains is the first obvious symptom of starch degradation. The coincident occurrence of small gaps between the vacuole and the interior of the amyloplast may allow leakage of vacuolar sap into this organelle. Evidence that the vacuole represents the lytic compartment of plant cells that contains hydrolytic enzymes has been largely established by Matile (1975). The products of hydrolase activity can, on the other hand, be released into the vacuole via these gaps. As long as they are small, digestion may be under control and homeostasis maintained. If this idea and the widely accepted idea that the sugars produced by starch lysis enter the nectar are true, then these sugars must pass at least two membranes – the tonoplast and the plasma membrane (plasmalemma). In contrast to the open access of the vacuolar sap to the interior of the amyloplasts, indicated by the present study, engulfing of the plastids by the vacuole and subsequent hydrolysis of starch in the vacuole were described in the floral nectaries of *Eccremocarpus saber* (Belmonte *et al.*, 1994) and

Cucumis sativus (Peng *et al.*, 2004), and in senescing French bean leaves (Minamikawa *et al.*, 2001).

Accumulation of the products of starch degradation in the vacuole may serve one more transient function. If the sugar concentration in the apoplast of the nectary is at least 440 mM (see 'Solute flux necessary for nectar production'), a significant osmotic stress exists. These apoplastic solutes will lower cell turgor and cause plasmolysis. Transient local detachment of the protoplasts from the cell wall indicates such an event. As the toxic effect of prolonged plasmolysis will cause premature death, an increase in the solute concentration in the vacuole will counterbalance too much loss of water in order to facilitate extension growth of the NCs by enlargement of the vacuole, and provide adequate turgor for effective PCD, which is a slowly proceeding process (van Doorn and Woltering, 2005).

(d) Nuclear changes. Deformation of the nuclei and gradual disappearance of chromatin were found in this study to be relatively early symptoms of nuclear degradation. Changes in nuclear shape were also observed in dying cells of the tapetum (Papini *et al.*, 1999) and the nucellus (Greenwood *et al.*, 2005). However, the ultimate breakdown is a relatively late event, just as in most senescing cells (Noodén and Leopold, 1988).

(e) Intensification of electron opacity. The increase in the osmiophilic properties of the cytoplasm, nucleoplasm and contents of the endomembrane system correlates with the occurrence of osmiophilic particles at the periphery of the protoplast, in the gaps between the cell wall and the plasma membrane, and in the intercellular spaces. Conclusive evidence for possible ontogenetical relationships between these events is missing, however. Characteristic increases in cytoplasmic density were also observed in the so-called dense cells of the *Arabidopsis thaliana* nectary (Zhu and Hu, 2002) and during early degeneration of the tobacco synergid (Huang *et al.*, 1993).

(f) Disintegration of the tonoplast. As degradation of the NT advances to its end point, tonoplast integrity is lost. Dissolution and subsequent release of hydrolytic enzymes into the vestiges of cytoplasma, which promote final cell death, are common features of plant PCD (Jones, 2000; Moriyasu and Klionsky, 2004; Noodén, 2004). Eventually total autolysis of the remaining cytoplasmic constituents ensues, ending with leakage of the catabolites into the apoplast (Lam, 2004), from which they may be loaded into the structurally intact phloem and exported to sinks elsewhere in the plant. The breakdown of the remaining mitochondria seems to coincide with the breakdown of the tonoplast. The lipid-like globules, whose origin and function are completely unknown, and the plasma membrane, are among the most persistent cellular components.

The fate of the cell walls of the NT

The breakdown of cellular contents is paralleled by the occurrence of wavy cell walls. This buckling is followed by further collapse of the NC corpses as a result of forces exerted by the swelling fruit. Ensuing nectar secretion degeneration and the collapse of NCs was also observed in *Glycine max* (Horner *et al.*, 2003) and *Hexisea imbricata* (Stpiczyńska *et al.*, 2005). Cell walls are typically not eliminated during PCD in plants (Mittler, 1998), and crushing, tearing or overgrowth of dead cells by their expanding neighbours is one of their fates (Beers, 1997). The fact that cell walls are not degraded may reflect an energetic budget that is too high (Gray and Johal, 1998) or the cell walls perform specialized functions such as mechanical support or water transport (Krishnamurthy *et al.*, 2000). We think that once the mission of the nectary is accomplished, it alters to a mode in which not only resource mobilization but also defence should be the most important goals for preservation of the next generation. The production of a physical barrier composed of compressed cell walls and collapsed intercellular spaces may inhibit the invasion of pathogens via the permanently open stomata into living parts of the ovary. Nectar clearly represents a preferred medium for bacterial and fungal growth (Fig. 3B), and the bacterial pathogen *Erwinia amylovora* is known to follow this route during infection (Buban *et al.*, 2003).

Future directions

PCD is usually regarded as a genetically encoded active process that performs a detectable function in the life of the plant (Gunawardena *et al.*, 2005). If nectary death is correctly interpreted as programmed, a genetic control can be expected. In this case nectaries could be excellent model systems for the study of fundamental cell death processes, because the whole natural period from maturity to death is relatively short. In particular the nectaries of species that lend themselves readily to genetic manipulation, mutagenesis or transformation, such as *Arabidopsis thaliana*, may be employed. Enlargement of the vacuoles in the postsecretory nectary of *Arabidopsis thaliana* (Davis, 1994) and the ultrastructural changes observed during degeneration of the NT (Zhu and Hu, 2002) seem to be hallmarks of PCD. Genetic analysis using arabidopsis mutants that show abnormalities in nectary morphology – as for instance the petal loss-1 (ptl-1) mutation (Bowman, 1994) – may provide clues to the molecular mechanisms underlying PCD in the nectary.

ACKNOWLEDGEMENT

We are indebted to Dr A. R. Davis for an excellent revision of the manuscript.

LITERATURE CITED

Assmann U. 1986. *Nektaruntersuchungen an* Digitalis purpurea *Beständen*. PhD Thesis, FB Biology, University of Marburg, Germany.

Barth I, Meyer S, Sauer N. 2003. PmSUC3: characterization of a SUT2/SUC3-type sucrose transporter from *Plantago major*. *The Plant Cell* **15**: 1375–1385.

Beers EP. 1997. Programmed cell death during plant growth and development. *Cell Death and Differentiation* **4**: 649–661.

Behnke H-D. 1991. Distribution and evolution of forms and types of sieve-element plastids in the dicotyledons. *Aliso* **13**: 167–182.

Behrens WJ. 1879. Die Nektarien der Blüten. *Flora* **62**: 2–11, 17–27, 49–54, 81–90, 113–123, 145–153, 233–247, 305–314, 369–375, 433–457.

Belmonte E, Cardemil L, Kalin-Arroyo MJ. 1994. Floral nectary structure and nectar composition in *Eccremocarpus scaber* (Bignoniaceae), a hummingbird-pollinated plant of central Chile. *American Journal of Botany* **81**: 493–503.

Bieleski RL. 1995. Onset of phloem export from senescent petals of daylily. *Plant Physiology* **109**: 557–565.

Bowman J. 1994. *Arabidopsis – an atlas of morphology and development.* New York, NY: Springer-Verlag.

Buban T, Orosz-Kovacs Z, Farkas A. 2003. The nectary is the primary site of infection by *Erwinia amylovora* (Burr.) Winslow *et al.*: a mini review. *Plant Systematics and Evolution* **238**: 183–194.

von Czarnowski C. 1952. Untersuchungen zur Frage der Nektarabsonderung. *Archiv für Geflügelzucht und Kleintierkunde* **1**: 23–44.

Dangl JL, Dietrich RA, Thomas H. 2000. Senescence and programmed cell death. In: Buchanan B, Gruissem W, Jones R, eds. *Biochemistry and molecular biology of plants*. Rockville, MD: American Society of Plant Biologists, 1044–1100.

Davis AR. 1994. Nectary morphology and anatomy. In: Bowman J ed. *Arabidopsis – an atlas of morphology and development.* New York, NY: Springer-Verlag, 172–177.

Davis AR, Peterson RL, Shuel RW. 1986. Anatomy and vasculature of the floral nectaries of *Brassica napus* (Brassicaceae). *Canadian Journal of Botany* **64**: 2508–2516.

Davis AR, Peterson RL, Shuel RW. 1988. Vasculature and ultrastructure of the floral and stipular nectaries of *Vicia faba* (Leguminosae). *Canadian Journal of Botany* **66**: 1435–1448.

van Doorn WG, Woltering EJ. 2005. Many ways to exit? Cell death categories in plants. *Trends in Plant Science* **10**: 117–122.

Durkee LT. 1983. The ultrastructure of floral and extra-floral nectaries. In: Bentley B, Elias T, eds. *The biology of nectaries*. New York, NY: Columbia University Press, 1–26.

Durkee LT, Gaal DJ, Reisner WH. 1981. The floral and extrafloral nectaries of *Passiflora*. I. The floral nectary. *American Journal of Botany* **68**: 453–462.

Eleftheriou EP, Hall JL. 1983. The extrafloral nectaries of cotton. II. Cytochemical localization of ATPase activity and Ca^{2+} binding sites, and selective osmium impregnation. *Journal of Experimental Botany* **34**: 1066–1079.

Eschrich W. 1953. Beiträge zur Kenntnis der Wundsiebröhrenentwicklung bei *Impatiens holstii*. *Planta* **43**: 37–74.

Fahn A. 2000. Structure and function of secretory cells. *Advances in Botanical Research* **31**: 37–75.

Figier J. 1971. Etude infrastructurale de la stipule de *Vicia faba* L. au niveau du nectaire. *Planta* **98**: 31–49.

Findlay N. 1988. Nectaries and other glands. In: Baker D, Hall J eds. *Solute transport in plant cells*. New York, NY: Longman Scientific and Technical, 538–560.

Findlay N, Mercer FV. 1971. Nectar production in *Abutilon*. II. Submicroscopic structure of the nectary. *Australian Journal of Biological Sciences* **24**: 657–664.

Frei E. 1955. Die Innervierung der floralen Nektarien dikotyler Pflanzenfamilien. *Berichte der Schweizerischen Botanischen Gesellschaft* **65**: 60–114.

Frey-Wyssling A, Agthe C. 1950. Nektar ist ausgeschiedener Phloemsaft. *Verhandlungen der Schweizerischen Naturforschenden Gesellschaft* **130**: 175–176.

Frey-Wyssling A, Häusermann E. 1960. Deutung der gestaltlosen Nektarien. *Berichte der Schweizerischen Botanischen Gesellschaft* **70**: 150–162.

Gaffal KP, Heimler W. 2000. Die Nektarien von herzglycosidhaltigen Rachenblütlern – eine Quelle der Speise für Götter mit Herzinsuffizienz? *Mikrokosmos* **89**: 129–138.

Gaffal KP, El-Gammal S. 2003. Nectar and honey analyses for prognosis of phloem transport of natural plant toxins? *Drogenreport* **16**: 9–13 [in German with Summary and Conclusions in English].

Gaffal KP, Heimler W, El-Gammal S. 1998. The floral nectary of *Digitalis purpurea* L., structure and nectar secretion. *Annals of Botany* **81**: 251–262.

Ge YX, Angenent GC, Wittich PE, Peters J, Franken J, Busscher M, *et al*. 2000. NEC1, a novel gene, highly expressed in nectary tissue of *Petunia hybrida*. *The Plant Journal* **24**: 725–734.

Gray J, Johal GS. 1998. Programmed cell death in plants. In: Anderson M, Roberts J, eds. *Arabidopsis*. Annual Plant Reviews. Boca Raton: CRC Press, 360–394.

Greenwood JS, Helm M, Gietl C. 2005. Ricinosomes and endosperm transfer cell structure in programmed cell death of the nucellus during *Ricinus* seed development. *Proceedings of the National Academy of Sciences of the USA* **102**: 2238–2243.

Gunawardena AHLAN, Sault K, Donnelly P, Greenwood JS, Dengler NG. 2005. Programmed cell death and leaf morphogenesis in *Monstera obliqua* (Araceae). *Planta* **221**: 607–618.

Halmágyi L, Gulyás S. 1970. Nektarium und Nektarproduktion der *Digitalis*-Arten. *Acta Biologica Szeged* **16**: 43–50.

Haritatos E, Medville R, Turgeon R. 2000. Minor vein structure and sugar transport in *Arabidopsis thaliana*. *Planta* **211**: 105–111.

Hiepko P. 1966. Zur Morphologie, Anatomie und Funktion des Diskus der Paeoniaceae. *Berichte der Deutschen Botanischen Gesellschaft* **79**: 233–245.

Horner HT, Healy RA, Cervantes-Martinez T, Palmer RG. 2003. Floral nectary fine structure and development in *Glycine max* L. (Fabaceae). *International Journal of Plant Sciences* **164**: 675–690.

Huang BQ, Strout WG, Russell SD. 1993. Fertilization in *Nicotiana tabacum* – ultrastructural organization of propane-jet-frozen embryo sacs in-vivo. *Planta* **191**: 256–264.

Huelskamp M, Schnittinger A. 2004. Programmed cell death in development of plant vegetative tissue (leaf and root). In: Gray J, ed. *Programmed cell death in plants*. Oxford: Blackwell Publishing, 106–130.

Jones AM. 2000. Does the plant mitochondrion integrate cellular stress and regulate programmed cell death? *Trends in Plant Science* **5**: 225–230.

Koch A. 1884. Über den Verlauf und die Endigungen der Siebröhren in den Blättern. *Botanische Zeitung* **42**: 401–411, 417–427.

Koteyeva NK, Vassilyev AE, Tarlyn N, Franceschi VR. 2005. On mechanisms of nectar secretion. *XVII International Botanical Congress*, Vienna, Austria, Abstract 10·3·4.

Krishnamurthy KV, Krishnaraj R, Chozhavendan R, Christopher FS. 2000. The programme of cell death in plants and animals – a comparison. *Current Science* **79**: 1169–1181.

Lalonde S, Wipf D, Frommer WB. 2004. Transport mechanisms for organic forms of carbon and nitrogen between source and sink. *Annual Review of Plant Biology* **55**: 341–372.

Lam E. 2004. Controlled cell death, plant survival and development. *Nature Reviews Molecular Cell Biology* **5**: 305–315.

Lichius JJ, Daniel M, Fingerhut T, Wärtgen T. 1990. Der Nektar von *Digitalis*. *Deutsche Apotheker Zeitung* **130**: 2191–2193.

McKeon TA, Gaffield W. 1990. Viewing stereopictures in three dimensions with naked eyes. *Trends in Biochemical Sciences* **15**: 412–413.

Marginson R, Sedgley M, Douglas TJ, Knox RB. 1985. Structure and secretion of the extrafloral nectaries of Australian acacias. *Israel Journal of Botany* **34**: 91–102.

Matile P. 1975. The lytic compartment of plant cells. Cell biology monographs, Vol. 1. Berlin: Springer-Verlag.

Matile P, Winkenbach F. 1971. Function of lysosomes and lysosomal enzymes in the senescing corolla of the morning glory (*Ipomoea purpurea*). *Journal of Experimental Botany* **22**: 759–771.

Minamikawa T, Toyooka K, Okamoto T, Hara-Nishimura I. 2001. Degradation of ribulose 1,5 biphosphate carboxylase oxygenase by vascular enzymes of senescing French bean leaves: immunocytochemical and ultrastructural observations. *Protoplasma* **218**: 144–153.

Mittler R. 1998. Cell death in plants. In: Locksin RA *et al*., eds. *When cells die*. New York, NY: Wiley-Liss, 147–174.

Mittler R, Cheung AY. 2004. Cell death in plant development and defense. In: Lockshin RA, Zakeri Z, eds. *When cells die II.* Hoboken, NJ: John Wiley & Sons, 99–121.

Moriyasu Y, Klionsky DJ. 2004. Autophagy in plants. In: Klionsky DJ, ed. *Autophagy*. Georgetown, TX: Landes Bioscience, 208–215.

Nepi M, Pacini E, Cresti L, Guarnieri M, Artese D. 2005. Nectar carbohydrate sources: facts and hypothesis. *XVII. International Botanical Congress*, Vienna, Austria, Abstract 10·3·6.

Neumüller O-A. 1979. *Römpps Chemie-Lexikon*, 8. Aufl. Stuttgart: Franckh'sche Verlagshandlung.

Noodén LD. 2004. *Plant cell death processes*. Amsterdam: Elsevier.

Noodén LD, Leopold AC. 1988. *Senescence and aging in plants*. San Diego, CA: Academic Press.

Oparka KJ, Gates P. 1981. Transport of assimilates in the developing caryopsis of rice (*Oryza sativa* L.): ultrastructure of the pericarp vascular bundle and its connection with the aleurone layer. *Planta* **151**: 561–573.

Papini A, Mosti S, Brighigna L. 1999. Programmed-cell-death events during tapetum development of angiosperms. *Protoplasma* **207**: 213–221.

Patrick JW, Zhang WH, Tyerman SD, Offler CE, Walker NA. 2001. Role of membrane transport in phloem translocation of assimilates and water. *Australian Journal of Plant Physiology* **28**: 695–707.

Peng Y-B, Lu YF, Zhang DP. 2003. Abscisic acid activates ATPase in developing apple fruit especially in fruit phloem cells. *Plant, Cell and Environment* **26**: 1329–1342.

Peng Y-B, Li Y-Q, Hao Y-J, Xu Z-H, Bai S-N. 2004. Nectar production and transportation in the nectaries of the female *Cucumis sativus* L. flower during anthesis. *Protoplasma* **224**: 71–78.

Pennell RI, Lamb C. 1997. Programmed cell death in plants. *The Plant Cell* **9**: 1157–1168.

Percival M, Morgan P. 1965. Observations on the floral biology of *Digitalis* species. *New Phytologist* **64**: 1–22.

Pleasants JM, Chaplin SJ. 1983. Nectar production rates of *Asclepias quadrifolia*: causes and consequences of individual variation. *Oecologia* **59**: 232–238.

Ranganath RM, Nagashree NR. 2001. Role of programmed cell death in development. *International Reviews of Cytology* **202**: 159–242.

Razem FA, Davis AR. 1999. Anatomical and ultrastructural changes of the floral nectary of *Pisum sativum* L. during flower development. *Protoplasma* **206**: 57–72.

Rogers HJ. 2005. Cell death and organ development in plants. *Current Topics in Developmental Biology* **71**: 225–261.

Rubinstein B. 2000. Regulation of cell death in flower petals. *Plant Molecular Biology* **44**: 303–318.

Sammataro D, Erickson EH, Garment MB. 1985. Ultrastructure of the sunflower nectary. *Journal of Apicultural Research* **24**: 150–160.

Sawidis T. 1991. A histochemical study of nectaries of *Hibiscus rosa-sinensis*. *Journal of Experimental Botany* **42**: 1477–1487.

Schnepf E. 1973. Sezernierende und exzernierende Zellen bei Pflanzen. In: Hirsch GC, Ruska H, Sitte P, eds. *Grundlagen der Cytologie*. Jena: Fischer, 461–477.

Schulz A. 1986. Wound phloem in transition to bundle phloem in primary roots of *Pisum sativum* L. I. Development of bundle-leaving wound-sieve tubes. *Protoplasma* **130**: 12–26.

Schulz A, Kühn C, Riesmeier JW, Frommer WR. 1998. Ultrastructural effects in potato leaves due to antisense-inhibition of the sucrose transporter indicate an apoplasmic mode of phloem loading. *Planta* **206**: 533–543.

Smith MT, Saks Y, van Staden J. 1992. Ultrastructural changes in the petals of senescing flowers of *Dianthus caryophyllus* L. *Annals of Botany* **69**: 277–285.

Spurr AR. 1969. A low-viscosity epoxy resin embedding medium for electron microscopy. *Journal of Ultrastructural Research* **26**: 31–43.

Stadler S. 1886. *Beiträge zur Kenntnis der Nektarien und Biologie der Blüten*. Berlin: Friedländer.

Stead AD, van Doorn WG. 1994. Strategies of flower senescence – a review. In: Scott RJ, Stead AD, eds. *Molecular and cellular aspects of plant reproduction*. Cambridge: Cambridge University Press, 215–237.

Stpiczyńska M, Davies KL, Gregg A. 2005. Comparative account of nectary structure in *Hexisea imbricata* (Lindl.) Rchb. f. (*Orchidaceae*). *Annals of Botany* **95**: 749–756.

Thompson MV, Holbrook NM. 2003. Scaling phloem transport: water potential equilibrium and osmoregulatory flow. *Plant, Cell and Environment* **26**: 1561–1577.

Tobe H, Hakki MI, Langhammer L. 1989. Floral nectary in *Medinilla magnifica*, an Old World Melastomataceae. *Botanische Jahrbücher für Systematik, Pflanzengeschichte und Pflanzengeographie* **111**: 57–62.

Turgeon R, Webb JA. 1976. Leaf development and phloem transport in *Cucurbita pepo*: maturation of the minor vein. *Planta* **129**: 265–269.

Vassilyev AE. 2003. Pocemu vydielajetsia nektar? O mechanizmie nectarovydielenija. *Botaniceskij Zurnal* **88**: 1–8.

Wang ZP, Deloire A, Carbonneau A, Federspiel B, Lopez F. 2003. An *in vivo* experimental system to study sugar phloem unloading in ripening grape berries during water deficiency stress. *Annals of Botany* **92**: 523–528.

von Wettstein R. 1889. Über die Compositen der österreichisch-ungarischen Flora mit zuckerabscheidenden Hüllschuppen. *Sitzungsberichte der Kaiserlichen Akademie der Wissenschaften in Wien. Mathematisch-naturwissenschaftliche Classe* **97**: 570–589.

Winter H, Huber SC. 2000. Regulation of sucrose metabolism in higher plants: localization and regulation of activity of key enzymes. *Critical Reviews in Plant Sciences* **19**: 31–67.

Wist J, Davis AR. 2006. Floral nectar production and nectary anatomy and ultrastructure of *Echinacea purpurea* (Asteraceae). *Annals of Botany* **97**: 177–193.

Wolswinkel P. 1985. Phloem unloading and turgor-sensitive transport: factors involved in sink control of assimilate partitioning. *Physiologia Plantarum* **65**: 331–339.

Wright KM, Roberts AG, Martens HJ, Sauer N, Oparka KJ. 2003. Structural and functional vein maturation in developing tobacco leaves in relation to AtSUC2 promotor activity. *Plant Physiology* **131**: 1555–1565.

Wu G-L, Zhang X-Y, Zhang L-Y, Pan Q-H, Shen Y-Y, Zhang D-P. 2004. Phloem unloading in developing walnut fruit is symplasmic in the seed pericarp, and apoplasmic in the fleshy pericarp. *Plant and Cell Physiology* **45**: 1461–1470.

Wykes GR. 1952. The influence of variations in the supply of carbohydrate on the process of nectar secretion. *New Phytologist* **51**: 294–300.

Zamski E. 1996. Anatomical and physiological characteristics of sink cells. In: Zamski E, Schaffer AA, eds. *Photoassimilate distribution in plants and crops: source–sink relationships*. New York, NY: Marcel Dekker, 283–310.

Zhu J, Hu Z-H. 2002. Cytological studies on the development of sieve element and floral nectary tissue in *Arabidopsis thaliana*. *Acta Botanica Sinensis* **44**: 9–14.

Zimmermann JG. 1932. Über die extrafloralen Nektarien der Angiospermen. *Botanisches Centralblatt/Beihefte 1. Abteilung* **49**: 99–196.